Dynamics of a coupled spin-vortex pair in dipolar spinor Bose-Einstein condensates

Tiantian Li,[1] Su Yi,[2,*] and Yunbo Zhang[1,†]
[1]*Institute of Theoretical Physics, Shanxi University, Taiyuan 030006, China*
[2]*State Key Laboratory of Theoretical Physics, Institute of Theoretical Physics, Chinese Academy of Sciences, P.O. Box 2735, Beijing 100190, China*
(Received 9 February 2016; published 4 May 2016)

The collisional and magnetic field quench dynamics of a coupled spin-vortex pair in dipolar spinor Bose-Einstein condensates in a double-well potential are numerically investigated in the mean-field theory. Upon a sudden release of the potential barrier the two layers of condensates collide with each other in the trap center with the chirality of the vortex pair exchanged after each collision, showing the typical signature of in-phase collision for the parallel spin-vortex phase, and out-of-phase collision for the antiparallel phase. When quenching the transverse magnetic field, the vortex center in the single-layered condensate starts to make a helical motion with oval-shaped trajectories and the displacement of the center position is found to exhibit a damped simple harmonic oscillation with an intrinsic frequency and damping rate. The oscillation mode of the spin-vortex pair may be tuned by the initial magnetic field and the height of the Gaussian barrier; e.g., the gyrotropic motions for a parallel spin-vortex pair are out of sync with each other in the two layers, while those for the antiparallel pair exhibit a double-helix structure with the vortex centers moving opposite to each other with the same amplitude.

DOI: 10.1103/PhysRevA.93.053602

I. INTRODUCTION

Multilayered structures with stacked vortices have been intensively studied in the past few years, as their simple structure combined with highly nontrivial dynamical properties makes them fascinating objects of research [1–12]. They also provide the possibility to store information by means of their chirality and polarity. As an ideal platform, a dipolar spinor Bose-Einstein condensate can form a coreless vortex spontaneously in a pancake-shaped trap as a result of the anisotropy of the magnetic dipolar-dipolar interaction (MDDI) [13–19]. At intermediate temperature, a time-dependent Hartree-Fock-Bogoliubov study [20,21] has shown that an anomalous vortex pair may be spontaneously generated in the anomalous fraction with the condensed atoms filling the vortex core, when phases corresponding to the singly charged vortex are imposed in the condensed and the anomalous components of the gas. In particular, if an axial Gaussian barrier is imposed upon the pancake-shaped trap, the condensate will be divided into two layers with parallel or antiparallel vortices in them for different barrier height [22], which resembles the trilayer films with a ferromagnetic-nonmagnetic-ferromagnetic (FNF) structure.

In fact, the collisional dynamics of two topological defects in the condensate has drawn great attention in recent years [23–29]. A quantum version of Newton's cradle has been observed in the arrays of trapped one-dimensional (1D) Bose gases by turning off the crossed dipole trap quickly, which is in the proximity of an integrable system [23]. Recently, an experiment on the collision of matter-wave solitons consisting of a degenerate gas of ^{7}Li atoms was explored by using a Gaussian laser beam to cut the condensate in half and then turning off the barrier quickly [24]. This would enable us to study collisions in a more controlled manner and provides an ability to further explore the transition between integrable and nonintegrable systems. Another experimental study [26,27] on the collisional dynamics of two half-quantum vortices in a highly oblate ^{23}Na Bose-Einstein condensate (BEC) is performed by means of a vortex-dipole generation technique based on a moving optical obstacle, which demonstrates the short-range interaction between half-quantum vortices with different core magnetizations. To understand the collisional dynamics of a spin-vortex pair [22] formed in the pancake-shaped dipolar spinor condensate needs a full three-dimensional numerical simulation, which may provide further insight into the face-to-face collisional dynamics of the spin vortex through the controlled formation of a parallel or antiparallel vortex pair in the two layers of condensate.

A more practical motivation of this study lies in that magnetic vortex oscillators have been investigated for use as tunable microwave generators for future wireless communication [30–32]. Hence a better understanding of the fundamental physical properties of multilayered vortex structure is urgent in order to improve their functionality. Recently, investigations of dynamically coupled magnetic vortices have been reported in pairs [33–38], trios [39], chains [38,40], and arrays [38,41–44] of microscale ferromagnetic disks and squares [45–52]. The spontaneous parallel and antiparallel spin-vortex pairs provide an ideal platform for simulating multilayer magnetic vortices, and a transverse magnetic field may be applied to displace the vortex centers [22] to achieve the similar spin structure in nanopillar devices [49]. Moreover, the coupled motion of vortices in a trilayer structure has been addressed by a time-resolved imaging technique with a scanning transmission x-ray microscope [4,48], which stimulates us to reveal the vortex dynamics in coupled layers of the condensate after quenching the transverse field to zero.

In consideration of the wide applications of magnetic vortices, in this paper we focus on the collisional and quench dynamics of the initial spin-vortex ground states in Ref. [22] by suddenly turning off either the potential barrier of the double well or the transverse magnetic field. The paper is organized as follows. In Sec. II, we introduce our model and briefly review

*syi@itp.ac.cn
†ybzhang@sxu.edu.cn

the ground-state properties of this system, which is necessary to understand the following discussions. The numerical results on the collisional dynamics are presented in Sec. III. In Sec. IV we study the magnetic field quench dynamics of the spin vortex for different phases. Finally, we summarize our findings in Sec. V.

II. FORMULATION

The dynamics of the spin-vortex pair formed in a dipolar spinor condensate is governed by the following set of Gross-Pitaevskii (GP) equations in the mean-field treatment:

$$i\hbar\frac{\partial\psi_\alpha}{\partial t} = (T + U + c_0 n)\psi_\alpha + g_F\mu_B\mathbf{B}_{\rm eff}\cdot\mathbf{F}_{\alpha\beta}\psi_\beta, \qquad (1)$$

where $\psi_\alpha(\mathbf{r})$ denotes the condensate wave function for the spin component $\alpha = 0, \pm 1$, $n(\mathbf{r}) = \sum_\alpha |\psi_\alpha|^2$ is the total density, $T = -\hbar^2\nabla^2/(2M)$ is the kinetic energy with M the atomic mass, and $U(\mathbf{r})$ is the trapping potential. The coefficient $c_0 = 4\pi\hbar^2(a_0 + 2a_2)/(3M)$ describes the spin-independent collisional interaction in the condensate with $a_{0,2}$ being the s-wave scattering length for two spin-1 atoms in the total spin channels 0 and 2, g_F is the Landé g factor of the atom, μ_B is the Bohr magneton, and $\mathbf{F}$ is the angular momentum operator. All spin-related interactions are collected into the last term in the way of an effective magnetic field,

$$\mathbf{B}_{\rm eff}(\mathbf{r}) = \mathbf{B}_{\rm ext} + \frac{c_2}{g_F\mu_B}\mathbf{S}(\mathbf{r}) + \frac{c_d}{g_F\mu_B}\int\frac{d\mathbf{r}'}{|\mathbf{R}|^3} \times\left[\mathbf{S}(\mathbf{r}') - \frac{3[\mathbf{S}(\mathbf{r}')\cdot\mathbf{R}]\mathbf{R}}{|\mathbf{R}|^2}\right] \qquad (2)$$

with $\mathbf{R} = \mathbf{r} - \mathbf{r}'$ and $\mathbf{B}_{\rm ext}$ the external magnetic field. Here, $\mathbf{S}(\mathbf{r}) = \sum_{\alpha\beta}\psi_\alpha^*\mathbf{F}_{\alpha\beta}\psi_\beta$ is the spin density, and c_2 and c_d characterize the spin exchange and dipole-dipole interaction, respectively.

The dipolar interaction in the condensate induces an interesting spin-vortex structure in the ground state for a pancake-shaped trap potential $U(\mathbf{r})$. To create a spin-vortex pair, a Gaussian barrier of height A and width σ_0 is imposed upon a highly anisotropic harmonic potential with aspect ratio λ, leading to a combined trapping potential $U(\mathbf{r}) = \frac{1}{2}M\omega_\perp^2(x^2 + y^2 + \lambda^2 z^2) + Ae^{-z^2/(2\sigma_0^2)}$ with $\omega_\perp$ the radial trap frequency. In experiment, one may choose a Gaussian laser beam to cut the condensate into two halves [24] and the system can be considered quasi-two-dimensional clouds of atoms, nearly free to move in the planes. The vortex pair could be with either parallel or antiparallel spin on the two sides of the barrier [22], and the spin structures of the ground state, denoted as PSVP and ASVP, respectively, are determined by the height of the Gaussian barrier A for a fixed barrier width σ_0 in the absence of an external magnetic field. The competition between the tunneling splitting of the two wells and the interlayer MDDI energy induces a phase transition between PSVP and ASVP phases. An increasing transverse magnetic field is found to remove the spin vortices sequentially before the condensate is fully polarized.

By preparing the system in the two distinct phases it is interesting to study the dynamics of a coupled spin-vortex pair by turning off either the barrier or the magnetic field, both of which are described by solving numerically the time-dependent GP equation, Eq. (1), with the help of the real-time propagation method. To study the dynamics of the coupled vortex pair, the initial states for the quench dynamics of the condensate are prepared in the spin-vortex state based on our previous work on the ground state of the system [22]. For ^{87}Rb, we take $c_2 = 0.01c_0$ and deliberately increase the dipole-dipole interaction (DDI) parameter to $c_d = |c_2|$ to accelerate the convergence of the numerical calculation as in Ref. [22]. In addition, we take the same parameters as in a previous study, i.e., total atom numbers $N = 5\times10^5$, $\omega_\perp = (2\pi)100$ Hz, $\sigma_0 = 0.65\ell_\perp$, and $\lambda = 6$ in our numerical calculation, and the dimensionless units are $\hbar\omega_\perp$ for energy, $\ell_\perp = \sqrt{\hbar/(M\omega_\perp)}$ for length, $\omega_\perp^{-1}$ for time, and $\ell_\perp^{-3/2}$ for the wave function, respectively. Enhancement of the DDI by increasing the number of particles only slightly changes the critical barrier height A^* between the ASVP and PSVP phases. For example, for $N = 5\times10^5$ adopted in this work, $A^* = 246\hbar\omega$, while for $N = 2\times10^5$ we have $A^* = 158\hbar\omega$. This, however, does not change the dynamics qualitatively. In fact, it was verified that the qualitative results can be reproduced by solely increasing N to 1×10^7 with c_d being that of the ^{87}Rb atom.

III. COLLISION DYNAMICS

In order to provide an experimentally discernible signature of the PSVP and ASVP phases, we study the collision dynamics of the spin-vortex pair by turning off the barrier quickly in a very short time once the pair is formed in the upper and lower planes; i.e., the system is prepared deliberately at the beginning in the ground state of the double well with $A = 100\hbar\omega_\perp$ and $300\hbar\omega_\perp$, respectively. The atoms suddenly find themselves at the classical turning points of the harmonic trap in the z direction and begin to accelerate towards the center. We carried out a full three-dimensional calculation of the collision dynamics, and the integrated density profiles are presented in Fig. 1 for two oscillation cycles. As a result, the Newton's cradle–like dynamics [23] is observed in our system, featured with distinct interference fringes and chirality exchange in the spin-vortex pair.

The two sheets of cloud collide with each other in the center of the trap twice each full cycle, for instance at $t = \tau/4$ and $3\tau/4$ with $\tau = 2\pi/\omega_z = 1.05\omega_\perp^{-1}$, as illustrated in Fig. 1. When they first meet, the atoms in the PSVP phase produce global interference patterns in the whole condensate, while those in the ASVP phase are stirred only in the central area. At this moment, the collisional interaction among the three components is the strongest so that the exchange of the particle number is reached most frequently. We find that the density of the spin-0 component n_0, defined as the full space integration of $|\psi_0|^2$, decreases during the first collision time for the PSVP phase, indicating that this phase favors a particle-exchange direction $2|0\rangle \to |1\rangle + |-1\rangle$, while it increases for the ASVP phase and an opposite particle-exchange channel is preferred. It is worthwhile to mention that the magnetization of the z axis, $M_z = \int d\mathbf{r}(|\psi_1|^2 - |\psi_{-1}|^2)$, remains zero in the whole evolution process so that the particle number density of $\pm$ components always satisfies $n_1 = n_{-1}$.

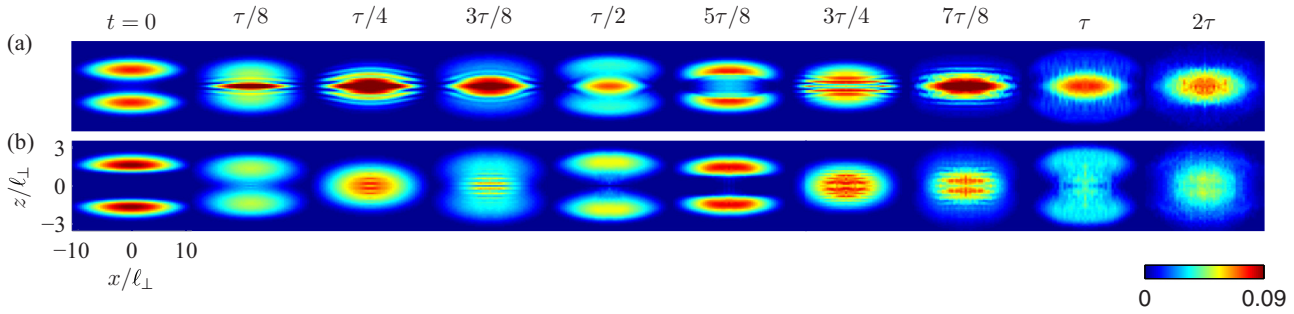

FIG. 1. Collision dynamics of a coupled spin-vortex pair in (a) PSVP ($A = 100\hbar\omega_\perp$) and (b) ASVP ($A = 300\hbar\omega_\perp$) phases of the condensate when the Gaussian barrier is turned off suddenly. Each image denotes the cloud density in the x-z plane after integrating along the y axis.

And then, the two layers of condensate pass straight through each other before reemerging on the other side. When the condensates separate into two parts again at $t = \tau/2$, we observed an interesting phenomenon that the chiralities of the spin-vortex pair in the upper and lower layers, i.e., the circulations of the in-plane magnetization components colored by red and blue in Fig. 2, exchange with each other in the ASVP phase and are restored at $t = \tau$ except that the spin structures are a little distorted near the vortex center, while those in the PSVP phase are the same as they should be. The phase differences between the lower and upper parts ϕ_0 (which is zero in the PSVP and π in the ASVP) leads to drastically different behavior in the wave functions: at the half period $t = \tau/2$ a density peak appears at the center of mass of the condensate for the PSVP case, indicating an in-phase collision, which is not observed for the ASVP case, implying an out-of-phase collision. These phenomena are in good agreement with the experimental observation of the collision of matter-wave solitons [24]. Different from the 1D collision, the face-to-face oscillation here in two dimensions will be destructed in a few cycles, which can be understood as a result of the density-dependent inelastic collision.

IV. QUENCH DYNAMICS OF THE TRANSVERSE MAGNETIC FIELD

The dynamics of magnetic vortices in nanodisks or multilayer structures manipulated by the magnetic field has attracted more and more attention [45–49]. The rotation of a vortex as a whole around its equilibrium position is found in a gyrotropic mode with a frequency far below the ferromagnetic resonance of the corresponding material [48]. Here we show a similar oscillation mode of the spin-vortex pair tuned by the magnetic field in the dipolar spinor condensate system. We focus on the motion of the vortex center in three typical structures, i.e., the single layer, PSVP, and ASVP, when the transverse field is suddenly quenched to zero. In the following we show the time-resolved trajectories of the vortex centers in the $z = z_{\min}$ plane with $z_{\min}$ being the positions of the potential minima along the z axis. In the three cases discussed here, we have $z_{\min} = 0$ for a single-layer condensate in a harmonic trap, and $z_{\min} = \pm\sigma_0\sqrt{2\ln(A/\lambda^2\sigma_0^2)}$ for the double-well structure.

Dynamics of a spin vortex in a single-layered condensate. We first consider the motion of the vortex center in a single-layered, pancake-shaped condensate starting from an initial state with a spin vortex for $B_x = 25\ \mu$G which may be regarded as a reference for more complex structures. As demonstrated in Fig. 3(a), when the field is removed quickly, the vortex center in the $z = 0$ plane starts to make a helical motion with an oval-shaped trajectory in the x-y plane. The projection of the center position on the y axis, that is, the displacement of the vortex center, is found to exhibit a well-defined periodic oscillation for quite a long time, as shown in Fig. 3(b). This gyrotropic motion of the vortex center has been fitted with a damped simple harmonic oscillation motion as $\Delta y(t) =$

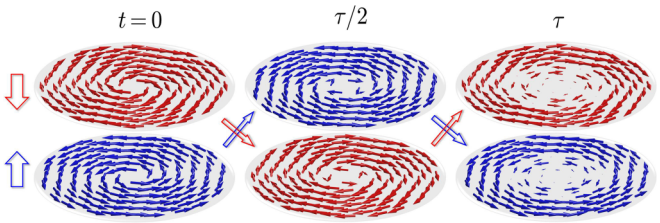

FIG. 2. Spin-vortex pair in the three collisional moments for the ASVP phase. Spin structures in the initial potential minima are shown in the upper and lower layers with the chiralities exchanged after each collision; the chiralities are inverted at $t = \tau/2$ and restored at $t = \tau$.

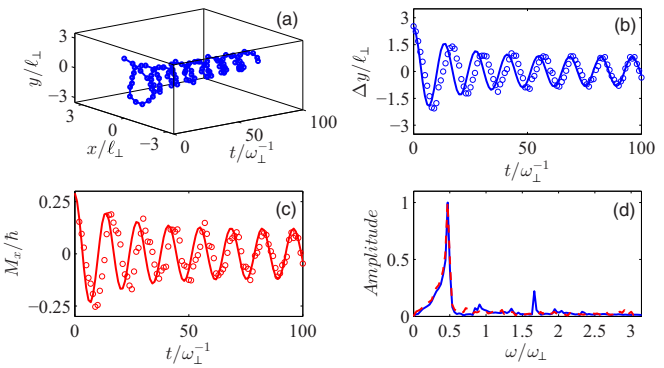

FIG. 3. Time-resolved trajectories of (a) the vortex centers in the $z = 0$ plane and (b) the displacement of the vortex center in the y axis when the transverse magnetic field ($B_x = 25\ \mu$G) is removed suddenly after initially preparing the system in the ground state of a harmonic trap. (c) The magnetization M_x shows similar oscillation behavior with the same characteristic frequency as can be seen from (d) the spectral analysis for the two signals. The solid lines in (b) and (c) are fitted with a damped simple harmonic oscillation.

$[y_0 \exp(-\beta t) + y_1]\cos(\omega_0 t)$, where $y_0 = 1.7\ell_\perp$, $y_1 = 0.8\ell_\perp$, $\beta = 5.84 \times 10^{-2}\omega_\perp$, and $\omega_0 = 0.46\omega_\perp$. This can be explained by taking into account the fact that the magnetic vortex is driven to move by a precessional torque generated by turning off the transverse magnetic field suddenly. We also examine the time dependence of the magnetization along the x axis, $M_x = \int d\mathbf{r} S_x(\mathbf{r})$, in Fig. 3(c). The oscillation there has been fitted with a formula $M_x(t) = [M_0 \exp(-\beta t) + M_1]\cos(\omega_0 t)$ with $M_0 = 0.17\hbar$ and $M_1 = 0.12\hbar$. We find that the characteristic damping parameter β and the oscillation frequency ω_0 match exactly with those in the evolution of the displacement of the vortex centers, $\Delta y(t)$. This can be clearly seen in the Fourier spectral analysis of the two oscillations in Fig. 3(d). During the evolution, however, the magnetizations along the y and z axes are found to be constantly zero.

Staring from a polarized state gives another scenario of the quench dynamics of the spin structure in a single-layered condensate, including the vortex formation and its helical motion. Figure 4 shows the details: four vortices are formed after the quench of the magnetic field, and they merged sequentially into two, and then to a single vortex. Meanwhile, the magnetization is found to undergo a rather slow damping oscillation. Once the vortex is stabilized, its center moves in just the same way as the helical motion with oval-shaped trajectory, the frequency of which tends to match the small transverse field case for $B_x = 25\ \mu$G as shown in the bottom panel in Fig. 4. We therefore conclude that the oscillation frequency of the vortex center in the single-layered condensate is intrinsic and irrelevant to the quenching initial state.

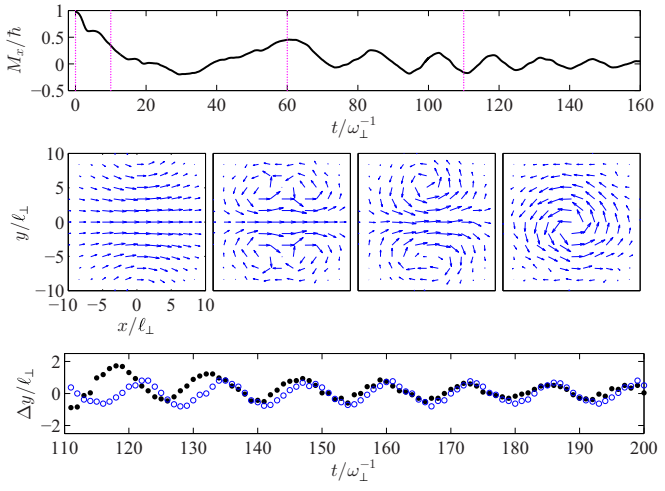

FIG. 4. Quench dynamics of the spin structure in a single-layered condensate staring from a polarized ground state with a transverse magnetic field $B_x = 70\ \mu$G. The top panel shows the time dependence of the magnetization along the x axis. The middle panels show the formation and stabilization of the spin vortex in the $z = 0$ plane at four evolution times $t = 0\omega_\perp^{-1}$, $10\omega_\perp^{-1}$, $60\omega_\perp^{-1}$, and $110\omega_\perp^{-1}$ (magenta dotted vertical lines in the upper panel), respectively. The solid circles in the lower panel show the displacement of the vortex center in the y axis after the stabilization of the spin vortex, and the open circles show the corresponding long time oscillation of the vortex center for $B_x = 25\ \mu$G in Fig. 3(b).

Dynamics of a spin-vortex pair in the PSVP and ASVP phases. For the PSVP or ASVP ground state, the number of spin vortices decreases from two to zero with a growing transverse field in the three stages of the magnetization process, i.e., double-vortex, single-vortex, and polarized states. We first examine a small transverse field with $B_x = 25\ \mu$G, in which case the spin-vortex pair is formed in two sheets of condensate with the same chiralities and the centers displaced along the same direction for the PSVP state, and with opposite chiralities and the two centers separated away along opposite directions for the ASVP state. Quenching this transverse field abruptly to zero, we find that the dynamics of the vortex centers is much different from that of a single-layered condensate due to the existence of a significant interplay between the interwell MDDI and tunneling splitting of the double-well potential. For the PSVP phase, the vortex centers of the two layers make a gyrotropic motion but out of sync with each other, as shown in Fig. 5(a) and their projection on the y axis in Fig. 5(b). Clearly the average position of the two vortex centers is not zero due to the frequency difference of the oscillations in the upper and lower layers [the green line in Fig. 5(b)]. We also examine the time dependence of the magnetization M_x in Fig. 5(c), where the magnetization in the two parts oscillates in the same way as the displacement of the vortex centers, just as what happens

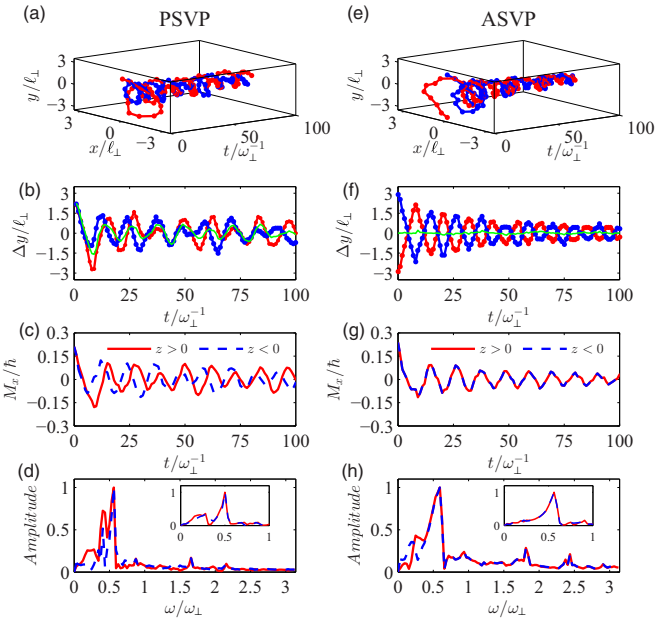

FIG. 5. Time-resolved trajectories of the vortex centers in the $z = z_{\min}$ planes (first row) and the displacement of the vortex center on the y axis (second row) when the transverse magnetic field ($B_x = 25\ \mu$G) is removed suddenly after initially preparing the system in the PSVP (left) and ASVP (right) phases, respectively. Panels in the third row show the time evolution of the corresponding magnetizations M_x in the upper ($z > 0$) layer and lower layer ($z < 0$), both of which oscillate in the same characteristic frequency as the motion of the vortex centers. The spectral analyses for the two signals are plotted in the bottom panels while the insets show the situation for a wider separation of the two layers, $\sigma_0 = 1.2\ell_\perp$. The red (blue) lines are for the upper (lower) layer and the green lines in the second row plot the average position of the two vortex centers.

in the single-layered condensate. In particular, we make a Fourier transform of the magnetization dynamics over a period of $100\omega_\perp^{-1}$ and find that for each layer a beat phenomenon appears in the dynamics with two slightly different characteristic frequency peaks as shown in Fig. 5(d). Further numerical simulations show that the weight of two frequencies in the dynamics changes along with the width of the Gaussian barrier. As the distance between the layers increases, the principle peak moves to higher frequency which represents the gyrotropic vortex motion, while the other peak corresponds to its higher harmonics. This can be understand as following: Note that both the interwell dipolar interaction (proportional to $1/\sigma_0^3$) and tunneling splitting (roughly proportional to $e^{-\widetilde{A}\sigma_0}$) decrease when the two layers are more widely separated at a fixed height of the interwell barrier $\widetilde{A}$ which is measured from the minima of the double-well potential. In the PSVP phase, the dipolar interaction inside each layer thus plays a major role so that the dynamics is dominated by a relatively strong nonlinear interaction as in the single-layer case with the principle characteristic frequency more prominently located at $0.50\omega_\perp$ for $\sigma_0 = 1.2\ell_\perp$, as can be seen in the inset of Fig. 5(d).

As forming an ASVP state needs a higher barrier A, the tunneling interaction between the two wells will be weakened so that the interwell dipolar interaction plays a key role in the process of the evolution. The trajectories of the vortex centers in the ASVP phase are shown in Fig. 5(e) and their projections in Fig. 5(f). We find that, starting from two opposite positions in the x-y plane, the two vortices with opposite chiralities exhibit a double-helix-structured gyrotropic motion and exhibit damped oscillation behaviors. It is worthwhile to notice that the motions of the vortex centers in the two layers are opposite to each other, but with the same amplitude, leading to a nearly zero average displacement of the vortex centers [the green line in Fig. 5(f)]. The magnetization M_x in each layer shows a perfect match during the damped evolution [Fig. 5(g)]. Obviously the beat phenomenon exists neither in the motion of vortex cores nor in the evolution of the magnetization M_x [Figs. 5(f) and 5(g)], just as in the single-layer case. The Fourier transform of the oscillation is a single-peaked spectrum with the characteristic frequency located at $0.56\omega_\perp$ for $\sigma_0 = 1.2\ell_\perp$ as shown in the inset of Fig. 5(h). The damping rate β of the oscillation can be adjusted with a varying barrier separation σ_0; for instance, it is three times faster for a closer space $\sigma_0 = 0.5\ell_\perp$ for which we have $\beta = 0.03\omega_\perp$ than for a wider separation $\sigma_0 = 1.2\ell_\perp$ for which we have $\beta = 0.01\omega_\perp$ with the fitting frequency $\omega_0 = 0.52\omega_\perp$.

Dynamics of a single vortex in the PSVP and ASVP phases. Next, we choose an intermediate magnetic field such that the initial state has a single vortex in, say, the lower layer, while the upper layer is polarized with $M_x(z<0) < M_x(z>0)$. Depending on the magnetic phases of the condensate, the system can support different combinations of vortex states. We compare the results for PSVP and ASVP in Fig. 6, which shows the time dependence of the magnetization M_x of the condensate for $A = 100$ and $300\hbar\omega_\perp$, $\sigma_0 = 0.65\ell_\perp$ after quenching the initial magnetic field $B_x = 50\ \mu$G for PSVP, and $B_x = 60\ \mu$G for ASVP, to zero. As we can see, the evolution here is similar to the single-layer case and can be divided into two stages: (i) a vortex formation stage (compared to the stabilization of the PSVP spin-vortex pair with the same chirality, it takes a little longer time for the two layers in the ASVP phase to form a spin-vortex pair with opposite chiralities) and (ii) a vortex oscillation stage (the centers of the stabilized vortices start to make the typical helical motion after $t = 25\omega_\perp^{-1}$ for PSVP and $t = 50\omega_\perp^{-1}$ for ASVP). We note that both the magnetization oscillation and the displacement of the vortex center are rather small for the PSVP phase, while those in the ASVP phase show quite a larger amplitude and lower frequency. Also, the two vortex centers in the ASVP phase follow the same trajectory as in Fig. 6(d), while the magnetizations in each layer are opposite to each other, leading to a nearly vanishing total magnetization as indicated by the black dash-dotted line in Fig. 6(b).

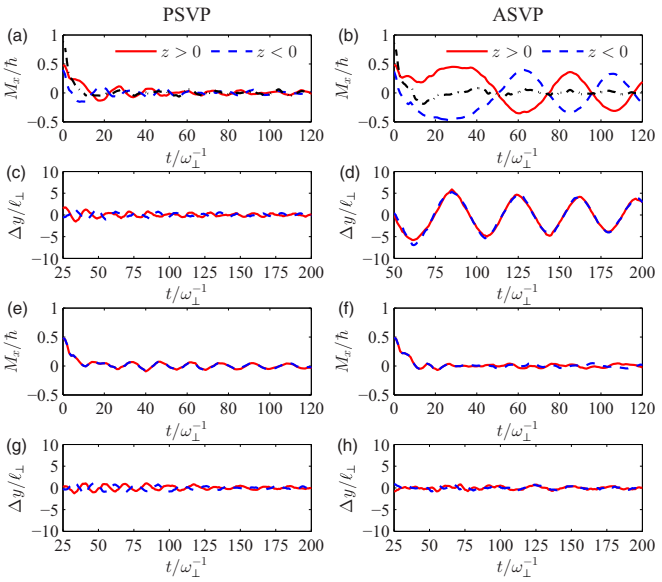

FIG. 6. Dynamics of a single vortex and a polarized state in the PSVP and ASVP phases. The time dependencies of the magnetization along the x axis are shown in (a), (b), (e), and (f) and the displacement of the vortex center on y axis in (c), (d), (g), and (h) for the PSVP case (left) and ASVP case (right), respectively, when the magnetic field is turned off suddenly. The corresponding initial transverse magnetic fields are $B_x = 60\ \mu$G for (a) and (c), 50 μG for (b) and (d), and 70 μG for (e)–(h).

Dynamics of a polarized state in the PSVP and ASVP. At last, we consider a polarized initial state in which all spins are polarized along the x direction at a large magnetic field $B_x = 70\ \mu$G. The fate of this state in a long time is a spin-vortex pair with opposite chiralities, irrelevant with the initial PSVP or ASVP phases. In this regime the magnetization in the two layers shows uniform behavior in both PSVP and ASVP phases, and in Figs. 6(e)–6(h) we still observe that the magnetization and the vortex centers of each layer oscillate with time for PSVP. In the ASVP phase, however, the oscillation is greatly suppressed, i.e., the vortex centers hardly move, with their centers pinned at the origin of the x-y plane once the vortices are stabilized. These features may be exploited to identify the individual configurations of PSVP and ASVP experimentally.

V. CONCLUSION

Before concluding, we would like to point out the connections of this study to the existing experimental works in some related fields. The appearance and dynamics of vortices and half vortices (HVs) in polariton condensates [28] and spin-1 antiferromagnetic condensates [26] are connected with spontaneous symmetry breaking and phase transitions. The cores of the primary half vortex in the polariton condensate are seen moving along orbital-like trajectories around the density maximum of the counterpolarized Gaussian state, keeping themselves orbiting during a few tenths of picoseconds, while the trajectories of the twin singularities upon full-vortex injection undergo a spiraling at large polariton densities. Such a dynamical configuration resembles the gyrotropic motions of the vortex center by manipulating the transverse field in double-layered dipolar condensate (see Fig. 5) and ferromagnetic nanodisks [47,48]. By means of *in situ* magnetization-sensitive imaging, pairs of half-quantum vortices with opposite core magnetization are generated when singly charged quantum vortices are injected into the easy-plane polar phase of an antiferromagnetic spinor Bose-Einstein condensate [26]. The separation distance of the pair and the magnitude of the core magnetization gradually saturate, which is consistent with the short-range repulsive interactions between half-quantum vortices with opposite core magnetization. In our system, both the displacement of the vortex center and the magnetization along the x axis exhibit well-defined periodic oscillation, which is attributed to the long-range dipole-dipole interaction in the condensate.

In conclusion, we have investigated the collisional and magnetic field quench dynamics of the coupled spin-vortex pair formed in a weakly interacting dipolar spinor BEC in a double-well potential. We show that, in the absence of a magnetic field, the two sheets of the cloud collide with each other with their chiralities exchanged after each collision, when the potential barrier is turned off suddenly. In particular, the evolutions of the vortex pair in PSVP and ASVP phases can be easily distinguished from the density distribution images at half of the oscillation period $\tau/2$ where the in-phase and out-of-phase collisions differ markedly depending on the relative phase between the upper and lower layers. Motivated by the experimental studies of the dynamics of magnetic vortices in nanodisks or multilayer structures, we subsequently study the quench dynamics of the vortex in the ground states of single- and double-layered condensates when the initial transverse field is removed quickly. The motion of the vortex center is found in a gyrotropic mode on account of the spin torque generated by quenching the transverse field. The displacement of the vortex center and the corresponding transverse magnetization are fitted with a damped simple harmonic oscillation motion with an intrinsic frequency and damping rate. These interesting dynamics provide an experimentally discernible signature of the PSVP and ASVP phases in the reach of current techniques of cold-atom experiments. In future works we intend to develop the non-zero-temperature theory to understand the effect of spin fluctuations and thermal magnons on the dynamics.

ACKNOWLEDGMENTS

This work was supported by the NSFC (Grants No. 11234008 and No. 11474189) and by the National 973 Program (Grant No. 2011CB921601), the Open Project Program of State Key Laboratory of Theoretical Physics, Institute of Theoretical Physics, Chinese Academy of Sciences, China (Grant No. Y5KF231CJ1). S.Y. acknowledges support from NSFC (Grants No. 11434011 and No. 11421063).

[1] K. Nakamura, T. Ito, and A. J. Freeman, Phys. Rev. B. **68**, 180404 (2003).
[2] S. D. Bader, Rev. Mod. Phys. **78**, 1 (2006).
[3] K. S. Buchanan, K. Y. Guslienko, A. Doran, A. Scholl, S. D. Bader, and V. Novosad, Phys. Rev. B **72**, 134415 (2005).
[4] K. W. Chou, A. Puzic, H. Stoll, G. Schütz, B. Van Waeyenberge, T. Tyliszczak, K. Rott, G. Reiss, H. Brückl, I. Neudecker, D. Weiss, and C. H. Back, J. Appl. Phys. **99**, 08F305 (2006).
[5] P. Vavassori, V. Bonanni, A. Busato, D. Bisero, G. Gubbiotti, A. O. Adeyeye, S. Goolaup, N. Singh, C. Spezzani, and M. Sacchi, J. Phys. D **41**, 134014 (2008).
[6] J. Wu, D. Carlton, E. Oelker, J. S. Park, E. Jin, E. Arenholz, A. Scholl, C. Hwang, J. Bokor, and Z. Q. Qiu, J. Phys. Condens. Matter **22**, 342001 (2010).
[7] J. Kurde, J. Miguel, D. Bayer, J. Sánchez-Barriga, F. Kronast, M. Aeschlimann, H. A. Dürr, and W. Kuch, New J. Phys. **13**, 033015 (2011).
[8] S. Wintz, T. Strache, M. Körner, M. Fritzsche, D. Markó, I. Mönch, R. Mattheis, J. Raabe, C. Quitmann, J. McCord, A. Erbe, and J. Fassbender, Appl. Phys. Lett. **98**, 232511 (2011).
[9] S. Wintz, T. Strache, M. Körner, C. Bunce, A. Banholzer, I. Mönch, R. Mattheis, J. Raabe, C. Quitmann, J. McCord, A. Erbe, K. Lenz, and J. Fassbender, Phys. Rev. B **85**, 134417 (2012).
[10] S. Wintz, C. Bunce, A. Banholzer, M. Körner, T. Strache, R. Mattheis, J. McCord, J. Raabe, C. Quitmann, A. Erbe, and J. Fassbender, Phys. Rev. B **85**, 224420 (2012).
[11] O. V. Sukhostavets, G. R. Aranda, and K. Y. Guslienko, J. Appl. Phys. **111**, 093901 (2012).
[12] A. A. Awad, A. Lara, V. Metlushko, K. Y. Guslienko, and F. G. Aliev, Appl. Phys. Lett. **100**, 262406 (2012).
[13] Y. Kawaguchi, H. Saito, and M. Ueda, Phys. Rev. Lett. **97**, 130404 (2006).
[14] L. Santos and T. Pfau, Phys. Rev. Lett. **96**, 190404 (2006).
[15] S. Yi and H. Pu, Phys. Rev. Lett. **97**, 020401 (2006).
[16] M. Takahashi, S. Ghosh, T. Mizushima, and K. Machida, Phys. Rev. Lett. **98**, 260403 (2007).
[17] S. Yi and H. Pu, arXiv:0804.0191.
[18] J. Zhang and T. L. Ho, J. Low Temp. Phys. **161**, 325 (2010).
[19] A. Hubert and R. Schäfer, *Magnetic Domains* (Springer, Berlin, 1998).
[20] A. Boudjemâa, Phys. Rev. A. **88**, 023619 (2013).
[21] A. Boudjemâa, Phys. Rev. A. **91**, 063633 (2015).
[22] T. Li, S. Yi, and Y. Zhang, Phys. Rev. A **92**, 063603 (2015).

[23] T. Kinoshita, T. Wenger, and D. S. Weiss, Nature (London) **440**, 900 (2006).
[24] J. H. V. Nguyen, P. Dyke, D. Luo, B. A. Malomed, and R. G. Hulet, Nat. Phys. **10**, 918 (2014).
[25] T. Yang, A. J. Henning, and K. A. Benedict, Laser Phys. **24**, 115502 (2014).
[26] S. W. Seo, S. Kang, W. J. Kwon, and Y. I. Shin, Phys. Rev. Lett. **115**, 015301 (2015).
[27] S. W. Seo, W. J. Kwon, S. Kang, and Y. Shin, arXiv:1512.07696.
[28] L. Dominici, G. Dagvadorj, J. M. Fellows, D. Ballarini, M. D. Giorgi, F. M. Marchetti, B. Piccirillo, L. Marrucci, A. Bramati, G. Gigli, M. H. Szymaska, and D. Sanvitto, Sci. Adv. **1**, e1500807 (2015)
[29] T. Kaneda and H. Saito, Phys. Rev. A **93**, 033611 (2016).
[30] V. S. Pribiag, I. N. Krivorotov, G. D. Fuchs, P. M. Braganca, O. Ozatay, J. C. Sankey, D. C. Ralph, and R. A. Buhrman, Nat. Phys. **3**, 498 (2007).
[31] A. Dussaux, B. Georges, J. Grollier, V. Cros, A. V. Khvalkovskiy, A. Fukushima, M. Konoto, H. Kubota, K. Yakushiji, S. Yuasa, K. A. Zvezdin, K. Ando, and A. Fert, Nat. Commun. **1**, 8 (2010).
[32] A. Ruotolo, V. Cros, B. Georges, A. Dussaux, J. Grollier, C. Deranlot, R. Guillemet, K. Bouzehouane, S. Fusil, and A. Fert, Nat. Nanotechnol. **4**, 528 (2009).
[33] S. Sugimoto, Y. Fukuma, S. Kasai, T. Kimura, A. Barman, and Y. C. Otani, Phys. Rev. Lett. **106**, 197203 (2011).
[34] S. Jain, H. Schultheiss, O. Heinonen, F. Y. Fradin, J. E. Pearson, S. D. Bader, and V. Novosad, Phys. Rev. B. **86**, 214418 (2012).
[35] A. Vogel, T. Kamionka, M. Martens, A. Drews, K. W. Chou, T. Tyliszczak, H. Stoll, B. Van Waeyenberge, and G. Meier, Phys. Rev. Lett. **106**, 137201 (2011).
[36] H. Jung, K. S. Lee, D. E. Jeong, Y. S. Choi, Y. S. Yu, D. S. Han, A. Vogel, L. Bocklage, G. Meier, M. Y. Im, P. Fischer, and S. K. Kim, Sci. Rep. **1**, 59 (2011).
[37] J. Shibata, K. Shigeto, and Y. Otani, Phys. Rev. B **67**, 224404 (2003).
[38] O. V. Sukhostavets, J. González, and K. Y. Guslienko, Phys. Rev. B **87**, 094402 (2013).
[39] X. Wang, D. J. Keavney, M. Asmat-Uceda, K. S. Buchanan, A. Melikyan, and X. M. Cheng, Appl. Phys. Lett. **105**, 102408 (2014).
[40] D. S. Han, A. Vogel, H. Jung, K. S. Lee, M. Weigand, H. Stoll, G. Schutz, P. Fischer, G. Meier, and S. K. Kim, Sci. Rep. **3**, 2262 (2013).
[41] A. Vogel, A. Drews, T. Kamionka, M. Bolte, and G. Meier, Phys. Rev. Lett. **105**, 037201 (2010).
[42] A. Barman, S. Barman, T. Kimura, Y. Fukuma, and Y. Otani, J. Phys. D: Appl. Phys. **43**, 422001 (2010).
[43] M. Hänze, C. F. Adolff, M. Weigand, and G. Meier, Appl. Phys. Lett. **104**, 182405 (2014).
[44] J. Shibata and Y. Otani, Phys. Rev. B **70**, 012404 (2004).
[45] W. Yu, P. S. Keatley, P. Gangmei, M. K. Marcham, T. H. J. Loughran, R. J. Hicken, S. A. Cavill, G. van der Laan, J. R. Childress, and J. A. Katine, Phys. Rev. B **91**, 174425 (2015).
[46] S. B. Choe, Y. Acremann, A. Scholl, A. Bauer, A. Doran, J. Stohr, and H. A. Padmore, Science **304**, 420 (2004).
[47] K. Yu. Guslienko, K. S. Buchanan, S. D. Bader, and V. Novosad, Appl. Phys. Lett. **86**, 223112 (2005).
[48] S. H. Jun, J. H. Shim, S. K. Oh, S. C. Yu, D. H. Kim, B. Mesler, and P. Fischer, Appl. Phys. Lett. **95**, 142509 (2009).
[49] V. Sluka, A. Kákay, A. M. Deac, D. E. Bürgler, C. M. Schneider, and R. Hertel, Nat. Commun. **6**, 6409 (2015).
[50] C. Phatak, A. K. Petford-Long, and O. Heinonen, Phys. Rev. Lett. **108**, 067205 (2012).
[51] B. V. Waeyenberge, A. Puzic, H. Stoll, K. W. Chou, T. Tyliszczak, R. Hertel, M. Fähnle, H. Brückl, K. Rott, G. Reiss, I. Neudecker, D. Weiss, C. H. Back, and G. Schütz, Nature (London) **444**, 461 (2006).
[52] K. Yamada, S. Kasai, Y. Nakatani, K. Kobayashi, H. Kohno, A. Thiaville, and T. Ono, Nat. Mater. **6**, 270 (2007).